A R C H I V E S O F M E T A L L U R G Y A N D M A T E R I A L S
Volume 59 2014 Issue 3
DOI: 10.2478/amm-2014-0163

M. WITKOWSKA*, A. ZIELIŃSKA-LIPIEC*, J. KOWALSKA*, W. RATUSZEK*

MICROSTRUCTURAL CHANGES IN A HIGH-MANGANESE AUSTENITIC Fe-Mn-Al-C STEEL

ZMIANY MIKROSTRUKTURALNE W WYSOKOMANGANOWEJ STALI AUSTENITYCZNEJ Fe-Mn-Al-C

Microstructural changes in the age-hardenable Fe-28wt.%Mn-9wt.%Al-1wt.%C steel during ageing at 550°C for various times have been investigated by transmission electron microscopy (TEM) and X-ray diffraction (XRD). The steel was produced in an induction furnace and the ingot, after homogenization at 1150°C for 3 hours under a protective argon atmosphere, was hot-rolled and subsequently cold-rolled up to 23% reduction. The sheet was then aged at 550°C for various times in an argon atmosphere and cooled in air. XRD analysis and TEM observations revealed a modulated structure and superlattice reflections produced by spinodal decomposition, which occurred during ageing at 550°C. The existence of satellites suggests that either $(Fe,Mn)_3AlC_x$ carbides were formed within the austenite matrix by spinodal decomposition during cooling or chemical fluctuactions occurred between the $(Fe,Mn)_3AlC_x$ carbides and the austenitic matrix.

Keywords: high-manganese austenitic steel, spinodal decomposition, carbides, microstructure

W pracy analizowano zmiany mikrostruktury w stali Fe-28%wt.Mn-9%wt.Al-1%wt.C zachodzące podczas starzenia w temperaturze 550°C w różnych czasach.

Stal Fe-28Mn-9Al-1C wytopiono w próżniowym piecu indukcyjnym. Po odlaniu wlewek homogenizowano w temperaturze 1150°C przez 3 godziny w atmosferze argonu. Wlewek walcowano na gorąco a następnie na zimno do 23 % odkształcenia. Próbki po odkształceniu starzono w temperaturze 550°C dla różnych czasów w atmosferze argonu i chłodzono na powietrzu.

Obserwacje elektronomikroskopowe starzonej stali Fe-28Mn-9Al-1C ujawniły modulowaną strukturę i refleksy od nadstruktury, co było efektem rozpadu spinodalnego, który miał miejsce podczas procesu starzenia. Występowanie satelitów na zapisach dyfrakcyjnych sugeruje, że węgliki $(Fe,Mn)_3AlC_x$ powstały w osnowie austenitycznej na skutek rozpadu spinodalnego zachodzącego podczas chłodzenia czy fluktuacji chemicznych występujących pomiędzy węglikami (Fe, $Mn)_3AlC_x$ i osnową austenityczną.

1. Introduction

High-manganese austenitic steels, of the general composition Fe-Mn-Al-Si-C, contain (in weight %), 12-35% manganese, 0-12% aluminium, 0-3% silicon and 0.05-1.3% carbon. Depending on the chemical composition, these high manganese steels are divided into [1-7]: Hadfield steels, containing from 1.1 to 1.3%C and from 12 to 13%Mn, TRIP (transformation-induced plasticity) steels containing from 0.05 to 0.15%C, from 15 to 22%Mn and Al and Si, TWIP (twinning induced plasticity) steels containing from 0.02 to 0.65%C, from 20 to 30%Mn, and Al; and TRIPLEX steels containing from 0.5 to 1.3%C, from 18 to 35%Mn, 8 to 12%Al and 3 to 6%Si. The microstructure of a TRIPLEX steel is composed of the austenitic γ-Fe(Mn, Al, C) solid solution matrix possessing a fine dispersion of nano-size κ-carbides $(Fe,Mn)_3AlC_{1-x}$ and α-Fe(Al, Mn) ferrite of varying volume fractions. These materials constitute a group of alloys of high strength and plasticity, and are also characterized by a smaller density in comparison with currently utilized steels. These alloys possess specific energy absorption values about 0.4 J/mm^3. Due to the above-mentioned characteristics, these steels constitute subsequent generations of materials, principally for the automotive and defense industries. Materials possessing such characteristics fulfill their functions well in the course of a possible collision of a vehicle, which ensures a higher level of safety. The microstructures and the mechanical properties of the austenitic Fe-Mn-Al-C alloys have been extensively studied [8-25]. In these studies, when a Fe-(28-35) wt.% Mn-(7-12) wt.% Al-(0.7-1.3) wt.% C alloy was solution treated, the microstructure was single – phase austenite. After ageing at temperatures from 500 to 750°C for moderate times, a fine modulated structure, of spinodal decomposition, results. This structure contains fine $(Fe,Mn)_3AlC$ carbides starting to precipitate coherently within the austenite matrix [12]. This κ carbidic phase has the ordered fcc structure ($L'1_2$). Due to the precipitation of $(Fe,Mn)_3AlC$ carbides within the austenite matrix, the strength of the alloy was remarkably increased without a significant loss in ductility. However, with increasing ageing time, the $(Fe,Mn)_3AlC$ carbides were found to precipitate, not only coherently within the austenite matrix (κ'), but

* AGH UNIVERSITY OF SCIENCE AND TECHNOLOGY, FACULTY OF METALS ENGINEERING AND INDUSTRIAL COMPUTER SCIENCE, AL. A. MICKIEWICZA 30, 30-059 KRAKÓW, POLAND

also heterogeneously on the γ/γ grain boundaries in the form of coarse particles (κ). There has been some disagreement in designation of the coherent metastable phase. In order to avoid confusion, a unified designation seems necessary. Han et al. [29] proposed κ' for the coherent metastable phase which forms prior to precipitation of the κ carbide. With increasing ageing time, within this temperature range, the coarse κ carbides grew into adjacent austenite grains through a $\gamma \rightarrow \gamma_0$ (carbon-depleted austenite)+κ carbide reaction+DO_3, a $\gamma \rightarrow \alpha$ (ferrite)+κ carbide reaction, a $\gamma \rightarrow \kappa$ carbide+β-Mn reaction, a $\gamma \rightarrow \alpha + \kappa$ carbide+β-Mn reaction, or a $\gamma \rightarrow \alpha + \beta$-Mn reaction, depending on the chemical composition and ageing temperature [11, 17, 21, 22].

The present work concerns the precipitation process of the $(Fe,Mn)_3AlC$ carbides in the high-manganese austenitic Fe-28Mn-9Al-1C steel after ageing at 550°C for various times.

2. Material and methods

A Fe-28Mn-9Al-1C ingot was prepared by vacuum induction melting and, after homogenization at 1150°C for 3 hours under a protective argon atmosphere, it was hot-rolled and next cold-rolled. Ageing was performed at 550°C for various times in an argon atmosphere. X-ray investigations, including phase analysis from the central layers of the sheets, were conducted on a Siemens D500 diffractometer, using Cu K_α radiation (λCuKα =1.54Å).

Transmission electron microscope (TEM) and scanning electron microscope (SEM) were used to observe microstructure and determine the phases in this steel. TEM samples were prepared by mechanical grinding the specimens to a thickness of 30μm and electropolishing with a double electropolisher (Tenupol-5, Struers^{TM}) at 10°C using a solution containing CH_3COOH (90 vol. %) and $HClO_4$ (10 vol. %). Electron microscope investigations were performed on longitudinal sections. For optical metallographic observations, specimens were mechanically, then electrolytically, polished and etched with a 5-10% Nital solution.

3. Results and discussion

The results of the X-ray diffraction analysis of the samples are presented in Figures 1 and 2. The X-ray phase analysis which has been conducted and the analysis of profiles of the diffraction lines make it possible to assess changes in the phase composition depending on the time of ageing. On the diffractogram (Fig.1) of the sample after 23% deformation, there appear peaks originating from the austenite phase. The strongest peak is that of austenite (220)γ, and those of austenite (111)γ, (200)γ and (311)γ are also a strong. After ageing, changes in the intensities of particular peaks were observed. The strongest peak became (111)γ, increasing with ageing time. This increase and the appearance of a peak originating from κ' – phase (550°C/96h, 550°C/192h) are illustrated in Fig. 1.

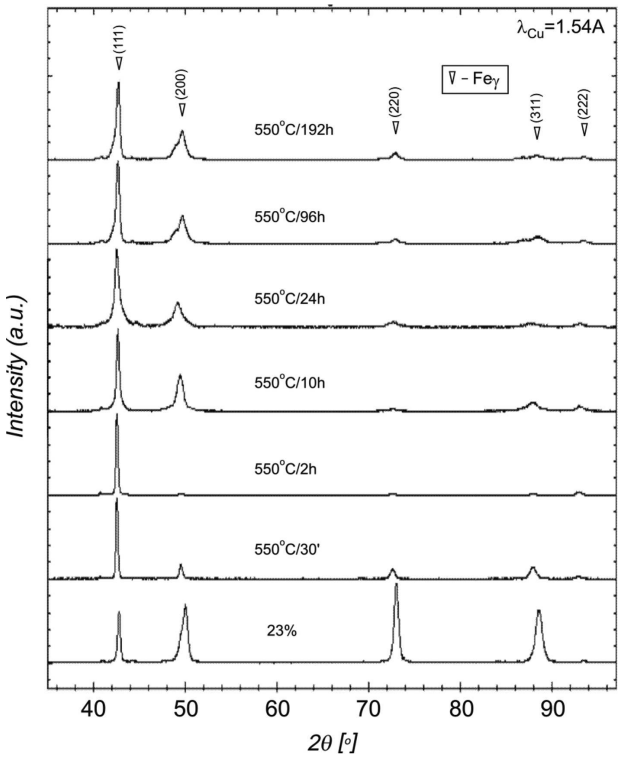

Fig. 1. X-ray diffraction patterns of the Fe-28Mn-9Al-1C steel after 23% reduction and ageing at 550°C for various times

More detailed analyses were carried out for the (200) peaks due to changes noticed in the samples during ageing. Figure 2 shows the X-ray diffraction profiles of the steel after cold-rolling and ageing at 550°C. The profile of the sample after 23% deformation reveals only a sharp (200)γ reflection, however specimens aged at 550°C for 96 and 192 hours showed a sideband reflection peak. The peak appearing on the low-angle side was the (200)κ' reflection of the C-rich κ' particles. The intensity of the (200)κ' peak increased with ageing time and the (200)γ and (200)κ' peaks shifted to smaller

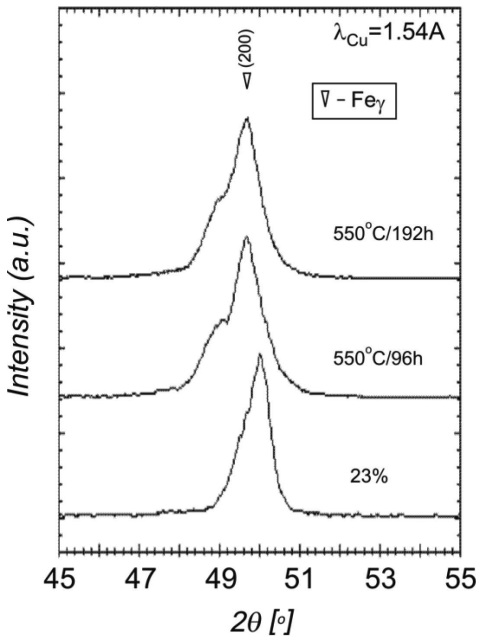

Fig. 2. X-ray diffraction profiles around the (200)γ Bragg reflection after rolling deformation and ageing at 550°C for 96 and 192 hours

TABLE 1
Experimental data obtained from the X-ray diffraction profiles of Fe-28Mn-9Al-1C steel after 23% of rolling deformation and ageing at 550°C for various times

State of material	Phase	23%	550°C/30'	550°C/2h	550°C/10h	550°C/96h	550°C/192h
Lattice parameter [nm]	κ'	–	–	–	3.7684	3.7319	3.7235
	γ	3.6460	3.6806	3.6791	3.6866	3.6688	3.6699
Misfit $\delta_{\kappa'-\gamma}$		–	–	–	0.0219	0.0170	0.0145
Wavelength [nm]		–	–	–	8.432	10.878	13.04
Elastic misfit a_0 =0.3652 [nm]		–	–	–	0.0318	0.0218	0.0196

Bragg angles. With increasing time, the sideband moved close to the main (200)γ peak.

The X-ray diffraction profiles data are shown in Table 1. The wavelength of the modulated structure was determined from the spacing between the sideband and the main (200) Bragg peak using the Daniel-Lipson equation [26]:

$$\lambda = \frac{ha_0 \tan\theta}{\Delta\theta(h^2 + k^2 + l^2)} \tag{1}$$

where λ = the average modulation wavelength,

a_0 = the lattice parameter of a homogeneous alloy,

θ = the Bragg angle for γ peak,

$\Delta\theta$ = the angular spacing between the sideband and the main (200) Bragg peak,

h, k, l = the Miller indices of the Bragg peak (h=2, k=0, l=0).

The wavelength λ of the modulated structure was calculated using equation (1). The misfit $\delta_{\kappa'-\gamma}$ was calculated using equation (2):

$$\delta_{\kappa'-\gamma} = 2\,|\,\frac{a_{\kappa'} - a_\gamma}{a_{\kappa'} + a_\gamma}\,| \tag{2}$$

From Table 1, it is clear that increasing the time of ageing made the wavelength increase.

The change of elastic misfit between γ_0 and κ' – phases $(a_{\kappa'} - a_{\gamma 0})/a_{\gamma 0}$, with ageing time is also given in Table 1. Together with increase in time of ageing, elastic misfit decreases, which is caused by the comparatively small contents of carbon.

The microstructures of the Fe-28Mn-9Al-1C steel after ageing at 550°C for various times are presented in Figures 4-6. After 23% deformation, austenite grains with twins are visible on Fig. 3.

After ageing at 550°C for 2 hours, the effects of deformation are still visible in the austenite grains. High density of dislocations and numerous bands were observed (Fig. 4a). The microstructure was very inhomogeneous and, only in small areas, were the initial stage of spinodal decomposition and the formation of a modulated structure observed (Fig. 4b).

The microstructure of the steel after ageing at 550°C for 96 hours is presented in Figure 5. It changed from a modulated (Fig. 5b) into a discrete two-phase microstructure: κ'+ solute depleted γ_0. Metastable coherent phase κ' may form by in situ transformation of the solute-enriched regions (Fig. 5b).

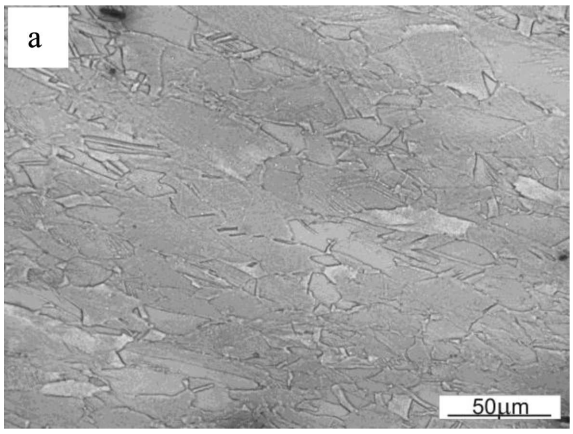

Fig. 3. An optical micrograph of specimen after 23% reduction

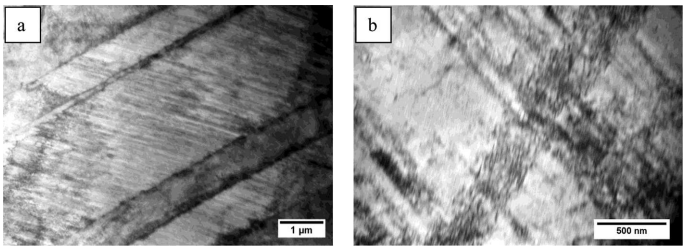

Fig. 4. TEM micrographs of the Fe-28Mn-9Al-1C steel after 23% reduction and ageing at 550°C for 2 hours (BF)

After this process, a raft-like arrangement of κ' precipitates in <100>γ directions was observed (Fig. 5c). Escalation of these decomposition leads to a very small dispersive (nanometric) precipitation of the κ'. The relation between γ and κ' phases is the cube on cube i.e. [100]γ|| [100]κ'. Stable κ-carbides precipitate heterogeneously on grain or twin boundaries (Fig. 5d). Extending the ageing time to 192 hours leads to increasing precipitation of the κ' carbide (Fig. 6). Moreover, a discontinous precipitation of κ carbides in the γ matrix at grain boundaries was observed (Fig. 6d). This reaction may be the result of the $\gamma \rightarrow \kappa' + \gamma_0 + DO_3$ transformation [17]. Increase in the precipitation of κ carbides on grain boundaries is accompanied, as a result of the $\gamma \rightarrow \kappa + \gamma_0$ transformation, in the formation of the orderly DO_3 phase, in accord with literature data [13, 17, 27, 28]. This phenomenon is confirmed by SEM observations of substantial precipitation of the κ carbide in the homogeneous phase.

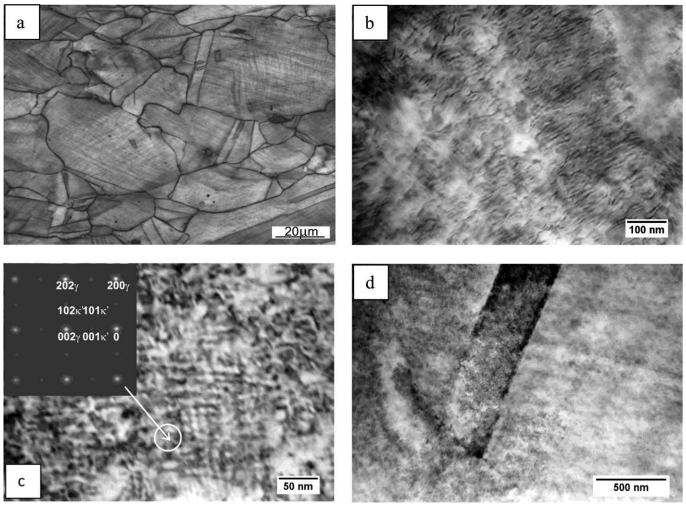

Fig. 5. Microstructures of the Fe-28Mn-9Al-1C steel after 23% reduction and ageing at 550°C for 96 hours (a) optical micrograph, b) TEM micrograph (BF), (c) TEM micrographs (BF) and diffraction pattern [100]γ|| [100]κ', d) TEM micrograph (BF)

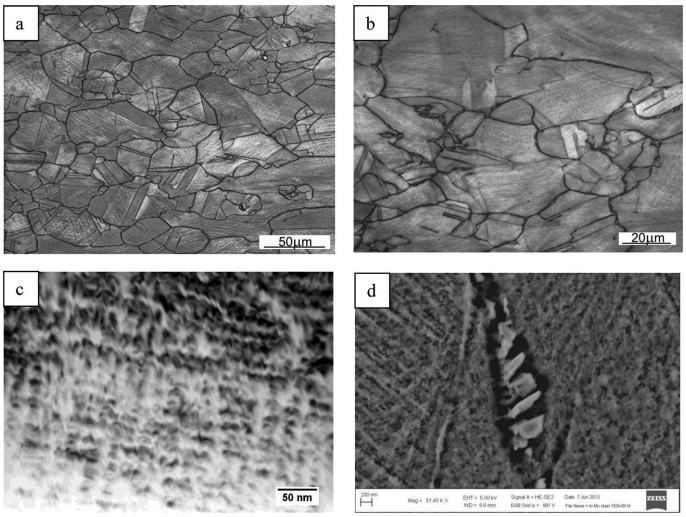

Fig. 6. Microstructures of the Fe-28Mn-9Al-1C steel after 23% reduction and ageing at 550°C for 192 hours (a, b) optical micrographs, (c) TEM micrograph (BF), (d) SEM micrograph

4. Conclusions

Phase analysis and microstructural observations showed that in the temperature 550°C for different times, spinodal decomposition and precipitation of the κ' phase occurs in Fe-28Mn-9Al-1C alloy. After cold rolling, it has a one phase structure of austenite with twins in some grains. After ageing at 550°C for 2 hours, the initial stage of spinodal decomposition was observed. The existence of satellites suggests that either the $(FeMnAl)_3C$ carbides were formed within the austenite matrix by spinodal decomposition during cooling or chemical fluctuactions occurred between the $(FeMnAl)_3C$ carbides and the austenite matrix. Extending the ageing time increased the average modulation wavelength and led to the precipitation of κ' $(FeMnAl)_3C$ carbides and the ordered DO_3 phase.

Acknowledgements

The work supported by the Polish Committee for Scientific Research under the contract 11.11.110. 157. The valuable contribution of Dr. Bogdan Rutkowski, of AGH-UST, to SEM studies is kindly acknowledged. Appreciation is also expressed to Prof. A.S. Wronski (University of Bradford, UK) for editing the manuscript.

REFERENCES

[1] G. Frommeyer, U. Brüx, P. Neumann, Supra-ductile and high-strengh manganes-TRIP/TWIP steels for high energy absorption purposes, ISIJ International, **43**, 438-446 (2003).
[2] S. Allain, J.P. Chateau, O. Bouaziz, S. Migot, N. Guelton, Correlation between the calculated stacking fault energy and the plasticity mechanism in Fe-Mn-C alloys, Mater. Sc. and Eng. **A387-389**, 158-162 (2004).
[3] O. Grässel, L. Krüger, G. Frommeyer, L. Meyer, High strength Fe-Mn(Al, Si) TRIP/TWIP steels development-properties-application, Inter. Jour. of Plast. **16**, 1391-1409 (2000).
[4] G. Frommeyer, U. Brüx, Microstructures and mechanical properties of high-strength Fe-Mn-Al-C light-weight TRIPLEX steels, Steel Research Int. **77**, 627-633 (2006).
[5] L.A. Dobrzański, A. Grajcar, W. Borek, Microstructure evolution and phase composition of high-manganese austenitic steels, Journal of Achievements in Materials and Manufacturing Engineering **31**, 218-225 (2008).
[6] J. Kowalska, W. Ratuszek, M. Witkowska, A. Zielińska-Lipiec, Influence of cold plastic deformation on the development of the texture in high-manganese austenitic steel, Solid State Phenomena **203-204**, 115-120 (2013).
[7] A. Ziewiec, E. Tasak, K. Ziewiec, K. Formowicz, Mechanical properties and microstructure of dissimilar material welded joint, Arch. Metall. Mater. **59**, 915 (2014).
[8] W.K. Choo, J.H. Kim, J.C. Yoon, Microstructural change in austenitic Fe-30.0wt%Mn-7.8wt%Al-1,3wt%C initiated by spinodal decomposition and its influence on mechanical properties, Acta Mater. **45**, 4877-4885 (1997).
[9] K. Sato, K. Tagawa, Y. Inoue, Modulated structure and magnetic properties of age-hardenable Fe-Mn-Al-C alloys, Metal. Trans. A **21A**, 5-11 (1990).
[10] K. Sato, K. Tagawa, Y. Inoue, Age hargdening of an Fe-30Mn-9Al-0.9C alloy by spinodal decomposition, Scripta Mater. **22**, 899-902 (1988).
[11] C.S. Wang, C.N. Hwang, C.G. Chao, T.F. Liu, Phase transitions in an Fe-9Al-30Mn-2.0C alloy, Scripta Mater. **57**, 809-812 (2007).
[12] I.S. Kalashnikov, O. Acselrad, A. Shalkevich, L.D. Chumakova, L.C. Pereira, Heat treatment and thermal stability of FeMnAlC alloys, J. Mater. Proc. Techn. **136**, 72-79 (2003).
[13] C.Y. Chao, C.H. Liu, Effects of Mn contents on the microstructure and mechanical properties of the Fe-10Al-xMn-1.0C alloy, Mater. Trans. **43**, 2635-2642 (2002).
[14] C.L. Lin, C.G. Chao, H.Y. Bor, T.F. Liu, Relationship between microstructures and tensile properties of an Fe-30Mn-8.5Al-2.0C alloy, Mater. Trans. **51**, 1084-1088 (2010).
[15] K.H. Han, W.K. Choo, Phase decomposition of rapidly solidified Fe-Mn-Al-C austenitic alloys, Metal. Trans. A **20A**, 205-214 (1989).

[16] K. Choi, C.H. Seo, H. Lee, S.K. Kim, J.H. Kwak, K.G. Chin, K.T. Park, N.J. Kim, Effect of aging on the microstructure and deformation behavior of austenite base lightweight Fe-28Mn-9Al-0.8C steel, Scripta Mater **63**, 1028-1031 (2010).

[17] C.Y. Chao, T.F. Liu, Phase transformations in an Fe-7.8Al-29.5Mn-1.5Si-1.05C alloy, Metal. Trans. A **24A**, 1957-1963 (1993).

[18] K. Sato, K. Tagawa, Y. Inoue, Spinodal decomposition and mechanical properties of an austenitic Fe-30wt.%Mn-930wt.%Al-0.930wt.%C alloy, Mater. Sci. Eng. **A111**, 45-50 (1989).

[19] G. Tsay, Y. Tuan, C. Lin, C. Chao, T. Liu, Effect of carbon on spinodal decomposition in Fe-26Mn-20Al-C alloys, Mater. Trans. **52**, 521-525 (2011).

[20] Y.H. Tuan, C.L. Lin, C.G. Chao, T.F. Liu, Grain boundary precipitation in Fe-30Mn-9Al-5Cr-0.7C alloy, Mater. Trans. **49**, 1589-1593 (2008).

[21] C.N. Hwang, C.Y. Chao, T.F. Liu, Grain boundary precipitation an Fe-8.0Al-31.5Mn-1.05C alloy, Scripta Mater. **28**, 263-268 (1993).

[22] C.Y. Chao, C.N. Hwang, T.F. Liu, Grain boundary precipitation an Fe-7.8Al-31.7Mn-0.54C alloy, Scripta Mater. **28**, 109-114 (1993).

[23] H. Springer, D. Raabe, Rapid alloy prototyping: Compositional and thermo-mechanical high throughput bulk combinatorial design of structural materials based on the example of 30Mn-1.2C-xAl triplex steels, Acta Mater. **60**, 4950-4959 (2012).

[24] J. Kowalska, W. Ratuszek, M. Witkowska, A. Zielińska-Lipiec, Development of microstructure and texture in Fe-26Mn-3Si-3Al alloy during cold-rolling and annealing, J. Alloys Comp. in press, http://dx.doi.org/10.1016/j.jallcom.2013.12.059

[25] B. Mikułowski, R. Zapała, J. Głownia, P. Wilk, Structure and properties of the centrifugally cast high-alloyed (25Cr35NiNbTi) steel after long-time operation in steam reforming. Arch. Metall. Mater. **58**, 785-790 (2013).

[26] V. Daniel, H. Lipson, An X-ray study of the dissociation of an alloy of copper, iron and nickel, Proc. Roy. Soc. **181**, 368-378 (1943).

[27] J.W. Lee, T.F. Liu, Phase transformations in an Fe-8Al-30Mn-1.5Si-1.5C alloy, Mater. Chem. and Phys. **69**, 192-198 (2001).

[28] C.C. Wu, J.S. Chou, T.F. Liu, Phase transformation in an Fe-10.1Al-28.6Mn-0.46C alloy, Metal. Trans A **22A**, 2265-2276 (1991).

[29] K.H. Han, K.C. Woong, Phase decomposition of rapidly solidified Fe-Mn-Al-C austenitic alloys, Metal. Trans A **20A**, 205-214 (1989).

Received: 15 September 2013.